Journal of Information Systems Engineering and Management

2025, 10(25s) e-ISSN: 2468-4376

https://www.jisem-journal.com/

Research Article

Experimental and Machine Learning-Based Investigation of Heat Transfer Enhancement in Interrupted Minichannels with CuO Nanofluid

I.H. Patel1*, A.G. Thakur2

^{1*}Department of Mechanical Engineering, SVPM's College of Engineering, India. ²Department of Mechanical Engineering, Sanjivani College of Engineering, Kopargaon, India.

ARTICLE INFO

ABSTRACT

Received: 29 Dec 2024 Revised: 14 Feb 2025 Accepted: 26 Feb 2025 This study experimentally investigates the influence of nanofluid concentration and minichannel geometry on convective heat transfer and pressure drop characteristics in minichannel heat sinks. A custom-designed test rig, incorporating precision flow control, calibrated thermal sensors, and a differential pressure transducer, was developed to ensure accurate thermal-hydraulic measurements. Six microchannel geometries-comprising both rectangular and V-type interrupted configurations-were fabricated using EDM and evaluated using CuO-water nanofluids prepared via a two-step synthesis method without surfactants. Results demonstrate that the V-type configuration consistently achieves superior heat transfer performance, as evidenced by higher Nusselt numbers, especially at elevated Reynolds numbers and nanoparticle concentrations. The optimal enhancement is observed at a 0.2% CuO concentration and V534 geometry, which strikes a favorable balance between increased heat transfer and manageable pressure drop. Uncertainty analysis confirms the robustness of the experimental data, with errors in heat transfer coefficient and Nusselt number maintained below 1.5%. Complementing the experiments, machine learning models were employed to predict thermal performance across various configurations. Gradient Boosting and Random Forest algorithms demonstrated high accuracy (R2 > 0.95) in predicting heat transfer coefficients and Nusselt numbers, validating their applicability for thermal optimization. The findings emphasize the critical role of channel geometry and nanoparticle concentration in designing efficient micro-scale thermal management systems, and highlight the potential of machine learning for predictive modeling and optimization in thermal engineering.

Keywords: Minichannel heat sink, Nanofluid, Machine Learning in Heat Transfer.

INTRODUCTION

The demand for efficient thermal management solutions has significantly increased due to advancements in microelectronics and compact electronic devices, which generate substantial heat fluxes. Traditional cooling methods often fall short in addressing the thermal management requirements of these high-performance devices. In recent years, minichannel heat sinks utilizing nanofluid have emerged as a promising technology due to their enhanced heat transfer capabilities and compact design. Nanofluids, formed by suspending nanoparticles in base fluids, exhibit improved thermal conductivity and convective heat transfer properties, making them attractive for micro-scale heat exchange applications. Key performance metrics evaluated include Nusselt number enhancement and associated pressure drop, aiming to identify optimal configurations that provide superior heat dissipation while maintaining manageable hydraulic performance.

LITERATURE REVIEW:

Shanmugam and Maganti [1] conducted experiments to analyze the thermal behavior of parallel microchannel heat sinks under non-uniform heat loads, using ML models like XGBoost which achieved R² = 0.98 for thermal response prediction. Sikirica [2] developed CFD-based surrogate models using neural networks and SHAP analysis, effectively optimizing microchannel designs with significant computational efficiency. Davoodabadi Farahani [3] assessed the influence of porous media, slip flow, and phase change materials on MCHS performance, achieving over 80% improvement verified through GMDH machine learning modeling. Aldaghi [4] applied a deep learning RL-GMDH model in a hybrid cooling setup using nanofluids and PCMs, demonstrating improved prediction and experimental performance. Wang [5] optimized finned microchannels using ANN to predict Nusselt number and pressure drop, achieving high prediction accuracy and optimal geometrical configurations. Aldaghi [6] also demonstrated the advantage of hybrid cooling (nanofluids + PCM + convection), resulting in significant thermal performance gains

Copyright © 2024 by Author/s and Licensed by JISEM. This is an open access article distributed under the Creative Commons Attribution License which permitsunrestricted use, distribution, and reproduction in any medium, provided the original work is properly cited.

(42.7% increase). Mieczkowski [7] used entropy generation minimization to optimize copper MCHS via genetic algorithms, lowering thermal losses and improving system reliability. Hamza [8] investigated nonlinear mixed convection in nanofluid films, highlighting the role of density variation in enhancing thermal transport under convective conditions. Li [9] proposed a twice-topology optimized heat sink that achieved a 46.16% Nusselt number increase and improved heat dissipation using image-based optimization. Kumar and Pandey [10] examined varying fin heights along microchannels, showing up to 32% thermal performance improvement, albeit with higher pressure drops. Zhang [11] analyzed twisted ribs in mini-channel heat sinks, identifying a 45° twist as optimal for balancing flow resistance and heat transfer.

Bouzennada [12] applied nanofluids in elastic-baffle microchannels and demonstrated improved cooling, particularly with bottom heating configurations. An [13] reviewed liquid metal-based heat sinks for high-temperature systems, identifying gallium-based coolants as superior in thermal conductivity. Feng [14] emphasized the necessity of twophase flow modeling in microchannels, improving prediction reliability for practical applications. Huang [15] addressed nanoparticle stability in hybrid nanofluids, recommending composite formulations to reduce sedimentation. Ghadhban and Jaffal [16] designed wave-channel multi-minichannel heat sinks, achieving better temperature uniformity with acceptable pressure loss. Noaman [17] found that structural features like ribs and curves enhanced thermal efficiency and flow mixing in modified microchannel configurations. Maghrabie [18] reviewed nanofluid integration in heat sinks, identifying hybrid particles and PCMs as effective performance enhancers. Zheng [19] investigated trapezoidal longitudinal vortex generators, which significantly improved heat transfer with minimal added pressure drop. Zhang [20] further validated the performance of twisted ribs in microchannels, optimizing geometry for thermal performance. Huang [21] proposed elliptical and triangular pin fins to mitigate nanoparticle deposition and maintain long-term thermal performance. Vafai [22] advocated for standardized testing and advanced simulations to close the gap between experimental and computational microchannel studies. Liu [23] explored the effects of nanoparticle concentration, finding an optimal range for enhancing convective performance. Khan [24] examined hybrid nanofluids, demonstrating their superior heat transfer capability, though at the cost of increased viscosity. Ali [25] showed that two-phase flow simulations yield more accurate thermal predictions than conventional single-phase methods. Wang [26] validated various microchannel geometries via CFD, optimizing shape for minimal thermal resistance. Chen [27] surveyed passive and active cooling strategies, highlighting PCMs and liquid metals as transformative for future designs. Lee [28] reviewed diagnostic techniques for microchannel heat sinks, advocating for micro-PIV and infrared thermography for accurate measurements.

Description Experimental Facility:

The experimental apparatus consists of a carefully designed setup equipped to supply a precisely metered working fluid. It is also capable of accurately measuring temperature, pressure, and flow rates within the system. K-type thermocouples are selected due to their high accuracy and suitable temperature measurement range, ensuring precise data collection.

TEST MANIFOLD DESIGN

This section discusses the design of the test manifold employed in the present experimental study. The test manifold is integrated within the test flow circuit and serves as structural support for mounting and securing the experimental device, facilitating precise fluidic and electrical connections.

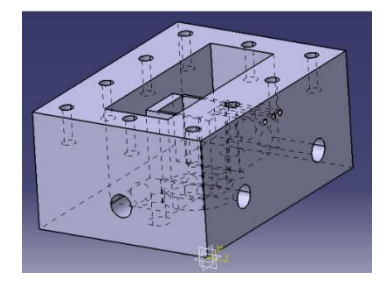


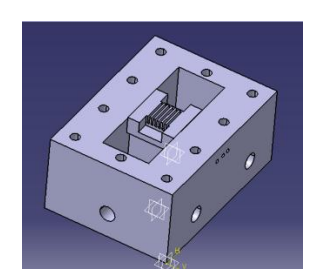
Figure 1: Test Manifold CAD Model

The test manifold as shown in fig 1 constitutes a component of the test section, serving as a platform to accommodate the electrical and fluidic connections. Manifold is manufactured with bakelite material as it is soft and non-conductive

and insulative material. Its purpose is to hold heat sink and provide cavity for inlet and outlet of water. Cavity for water is created with milling process. Inlet and outlet port was created with drilling process.

Heat sink:

Heat sink was manufactured with milling process. The hole for heater was created with drilling process. Slots are created with EDM process on heat sink. A slot size electrode was used for this process. The CAD model of heat sink is as shown in Figure 2a while heat sink with manifold (assembly) is as shown in Figure 2b below. The acrylic plate is used as top cover so that the flow will be visible from top side. The acrylic plate is sealed with manifold with screws and rubber oil seals so that there should not be any leakage of water from the joints. The heat sink incorporates microchannels, an integrated heater, and temperature sensors. In the present investigation, six distinct microchannel configurations have been examined. Each channel has a uniform length of 25 mm and a width of 0.53 mm, with the total number of channels fixed at ten.



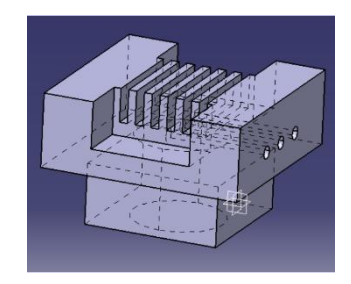


Figure 2 a: Heat Sink CAD Model

Figure 2 b: Heat sink with manifold CAD Models

The heater input current is accurately controlled to attain a specified heat flux of 32,000 W/m² throughout the experimental procedures. To validate constant heat flux temperature sensors are placed at the bottom of the heat sink wall. The spacing between each sensor is 5mm. So in 15 mm length the position of sensors is as follows; one at 0 (beginning of Channel), 5, 10, 15(end of channel). These sensors measured temperature of wall of channel.

Figure 2a shows test section with manifold. The test section aluminium heat sink with dimensions 25.4mm x 25.4 mm is placed exactly at centre of manifold; this heat sink has three side hole for sensors which measure temperature of heat sink at base. Here K- type thermocouples are used to record the temperature of wall. At the base of heat sink Nichrome heater is placed. To avoid heat loss from heater to surrounding asbestos insulation sheet is used. The top of heat sink is covered with transparent acrylic sheet so that it can facilitate the flow visualization. Temperature of water at inlet (before heat sink) and outlet (after heat sink) is measure with PT-100 temperature sensors. For experimentation total six minichannels were fabricated with different interrupted channel hydraulic diameters: 300 µm, 339µm, 534µm for Rectangular type and V shape Type geometries of interrupted chambers. Pressure taps are incorporated within the inlet and outlet manifolds to facilitate the measurement of pressure drop across the test section. The differential pressure transducer (Honeywell Make) is used to measure pressure drop across heat sink. Pressure taps are provided in the inlet and outlet manifolds for measurement of pressure drop across minichannels. The universal data logger is used to capture the reading of all temperature sensors used in experimental setup.

Nichrome strip type heater with input power 20 W is used for experimentation. K-Type temperature sensors are positioned at entrance and then at 5 mm equidistance from the inlet side, respectively, to measure the wall temperature. To measure fluid (water) three temperature sensors (PT-100-type) are placed from top of acrylic sheet. These sensors are 5mm before and after of the heat sink. One temperature sensor used to measure inlet fluid temperature while other two measure outlet fluid temperature as shown in Figure 3.A flat heater is placed at bottom of the heat sink. Two sensors are placed at 5 mm away from heat sink to measure outlet temperature of water. One sensor is placed at 5 mm away from heat sink to measure inlet temperature of water. These three sensors which are used to measure water temperature are inserted from top acrylic in manifold.

Experimental Apparatus and procedure

The experimental apparatus employed for evaluating the performance of the minichannels is illustrated in Figure 3.

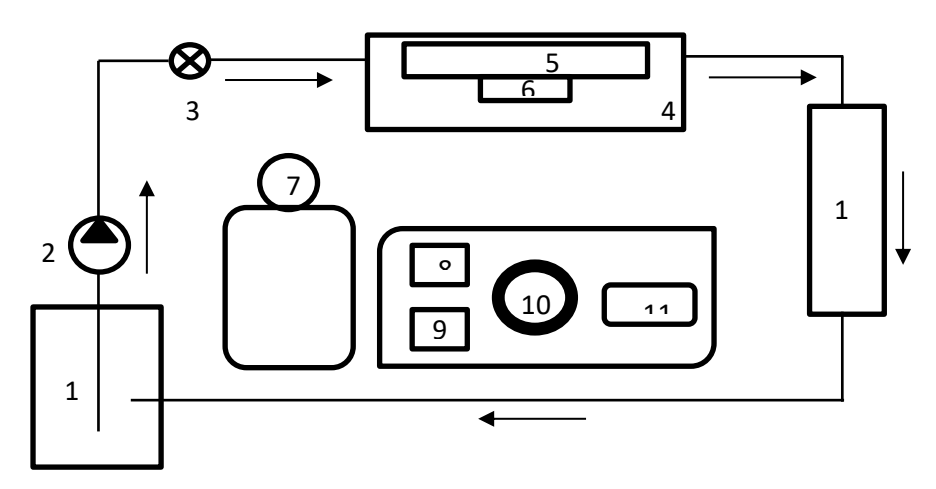


Figure 3 a Experimental Setup

1-Water Reservoir, 2-Micropump, 3-Flow meter, 4-Test section, 5-Test heat sink , 6-Heating element,7-Pressure measuring transducer, 8-Voltmeter, 9- Ammeter,10-Dimmer statt,11-Data logger, 12- Shell and tube type Heat Extractor



Figure 3 b Actual Experimental Setup

The experimental setup includes reservoir of water, micro pump, filter, manifold, heat sink, heater, voltmeter, ammeter, dimmer stat, data logger and heat exchanger. A storage tank of 20 litre capacity is used to store water for experimentation. The micropump is used to pump water. This micro pump used to give least flow of 0.0016 l/m, which is required for low Reynold number. There is possibility of any contamination in the water which can block channels so we use filter of 70 μ m before channel entry. The frequency of replacing the filter mesh every 15 days which means that the filter mesh should be removed, cleaned, or replaced with a new one every two weeks to prevent it from becoming clogged or fouled. This is important because a clogged filter can lead to decreased efficiency or even damage to the system. The nanofluid enters through the manifolds, which are positioned in alignment with the heat sink. The Manifold has two bell shape cavities. One at entrance of heat sink and another at exit of heat sink.

The bell shape cavity provides smooth entrance of water in minichannels. Due to this feature of bell shape cavity the water gets stabilize in manifold. Once nanofluid comes in contact with minichannels, it absorbs heat from minichannels and it becomes warm and flows to the outlet bell shape cavity of manifold. Shell and tube heat exchanger is used to cool nanofluid to ambient temperature so that it can recirculate in a loop.

Parametric variation Details of Minichannels:

The dimensional details of minichannels used for experimentations in the current work are given below in table 1

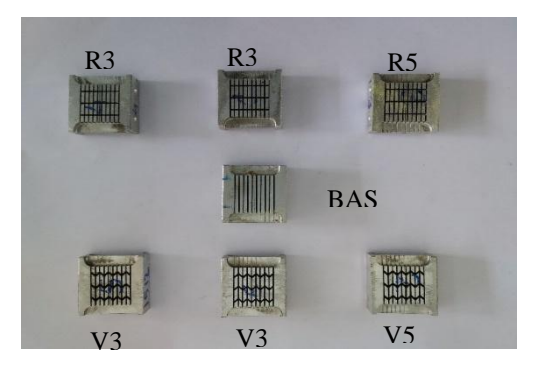
| No. of | Width | Height(b) | Width of interrupted | Length(L) | Hydraulic Diameter |
|----------|-------|-----------|----------------------|------------|--------------------|
| Channels | (w)µm | μm | Channel(c) μm | mm | (Dh) μm |
| 10 | 534 | 2910 | 300 | 25.4 | 903 |
| 10 | 534 | 2910 | 339 | 25.4 | 903 |
| 10 | 534 | 2910 | 534 | 25.4 | 903 |

Table1: The dimensional details of minichannels

Fabrication of Minichannel Heat sink and Test Manifold:

The conventional (straight geometry) minichannels are fabricated using the wire-cut electrical discharge machining (EDM) method, while the interrupted channels require a two-step process. In the first step, an electrode of copper material is made using the wire-cut electrical discharge machining (EDM) method; identical in shape with the interrupted channel. In the second step, this copper electrode is utilised in the subsequent process of electric discharge machining to create interrupted channels in the desired shape.

The milling process is used for manifold with Bakelite material. After the manufacturing process, the heat sink dimension is measured using digital Vernier calipers and an electronic microscope. The accuracy of the EDM is ±0.005 mm in the manufacturing process. The various heat sinks tested in the present study are as shown in figure 5. Heat Sink with manifold is shown in Figure 6.





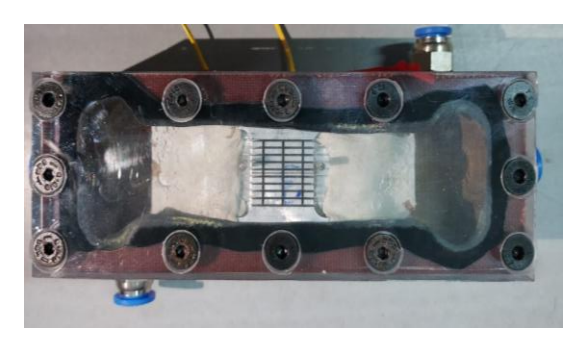


Figure 5: Heat sink with manifold

Preparation of Nano fluid and Experimentation

Two methods are used for preparation of nano fluid. The single step method may be more efficient and cost-effective since it combines the production of nanoparticles and their dispersion into the base fluid in a single step. However, this method may require specialized equipment and can be more challenging to control the size and distribution of the nanoparticles. On the other hand, the two-step method, as used in the current study, involves using presynthesized or purchased nanoparticles and adding them to the base fluid. This method may offer more control over the size and distribution of the nanoparticles and may not require specialized equipment. However, it may be more time consuming and expensive due to the cost of purchasing the nanoparticles. It is also important to consider the properties of the nanoparticles and the base fluid being used to prepare the nano fluid. The size, shape and surface chemistry of the nanoparticles can affect their dispersion and stability in the base fluid, as well as their thermal and electrical properties.



Figure 6: Cupric Oxide Nanopowder

The properties of the base fluid, including viscosity, heat carrying capacity can also impact the properties of the resulting nano fluid. The current study uses commercially available copper oxide nano-powder with a mean diameter of 40 nm to prepare a nanofluid with water as the base liquid. The amount of nanoparticles needed to achieve a 0.1% and 0.2% volume concentration solution is calculated. To create a uniformly dispersed solution, nanoparticles are disseminated in the pure water and stirred for 90 minutes with a magnetic stirrer. In this study surfactant or acid is not added to the nanofluid due to their potential to alter the thermo-physical properties of the nanofluid.

Additionally, adding acid could potentially damage the material due to its corrosive tendencies. Properties of nanofluid are calculated from the following equations (1 to 4) which will be used for calculation of heat transfer enhancement from nanofluid.

Density of nanofluid:

$$\mathcal{E}_{nf}(1)_{bf\ p} \tag{1}$$

Where ϕ is the nanoparticle volume fraction.

Heat carrying capacity:

$$C_{pnf} = \frac{(1)(C_{p,f})_{bf}(C_{p})_{p}}{\mathbb{E}_{nf}}$$
 (2)

Viscosity of Fluid

$$\kappa_{nf} = \frac{1}{k_p + (n-1)k_{bf} + \phi(\kappa_{bf} - k_p)}$$

 $K_{nf} = \frac{k_{\rho} + (n-1)k_{bf} - (n-1)_{bf}k_{\rho}}{k_{\rho} + (n-1)k_{bf} + \phi(\kappa_{bf} - k_{\rho})}$ Where, respectively, k_{p} , k_{bf} , and k_{nf} represent the thermal conductivity of a nanoparticle, base fluid, and nanofluid. The empirical form factor n for spherical nanoparticles is 3.

Validation of Experimental Setup:

In the reviewed open literature, it is noticed that very little work is available for minichannel. One of such work is reported by Lee and Garimella which contains results of Nusselt number enhancement. Therefore, this work is selected to validate experimental setup and procedure adopted in current research. The microchannel heat sink given in the work reported by Lee and Garimella has channel width of, a = 0.534 mm, Depth of channel, b = 2.91 mm, Number of channels, n= 10 was manufactured with wire cutting method and was tested experimentally for heat transfer. The results of Nusselt number as a function of Reynolds number are shown in Figur 7

Table 1: Specifications of Lee and Garimella[29]

| Test sections | Number of micro channels | width 'a' (μm) | Depth 'b' (μm) | Length (mm) | Hydraulic diameter 'Dh' (μm) | a (=b/w) |
|------------------|--------------------------|-------------------|----------------|-------------|---------------------------------|-------------|
| 1 | 10 | 194 | 884 | 25.4 | 318 | 4.56 |
| 2 | 10 | 229 | 1250 | 25. | 4 387 | 5.46 |
| 3 | 10 | 300 | 1520 | 25.4 | 501 | 5.07 |
| 4 | 10 | 339 | 1895 | 25.4 | 575 | 5.59 |
| 5 | 10 | 534 | 2910 | 25.4 | 903 | 5.45 |

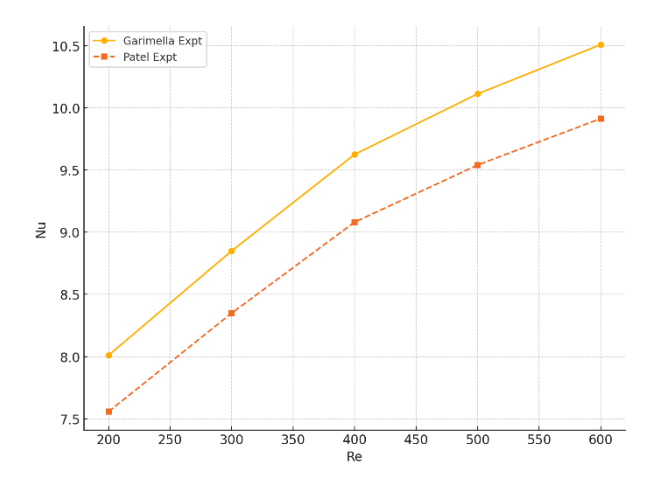


Figure 7: Nu vs Re Validation of Experimental Setup

The results obtained in the current work for geometry adopted from Lee and Garimella[29] with the procedure of current work agreed well within the range of 1% Nusselt number.

Uncertainty Analysis:

The experimental uncertainties in minichannel heat sinks can become significantly large due to the relatively small magnitude of measured parameters. Additionally, error propagation throughout the measurement system may pose considerable challenges, further compounded by the small physical dimensions of the tested components. Consequently, careful consideration and precise instrumentation are essential to mitigate these uncertainties and enhance the reliability of experimental results. Measurement instruments' percentage error includes temperature sensors, voltmeters, ammeters, stopwatches, pressure transmitters, and other measuring devices are 0.35, 0.1, 0.1, 0.1, 0.125 and 0.05 respectively are reported with calibrations done. The percentage of calibrated error by uncertainty analysis was found to be 0.99% in the heat transfer coefficient and 1.22% in Nu, for Pressure drop and Reynolds number the same was 0.17 % and 0.5% respectively.

RESULTS AND DISCUSSION:

Seven minichannels geometry (with three rectangular, three V type and basic straight heat sinks) heat sink were experimentally tested with Cu-O nanofluid as working medium. The experiment with these heat sink were carried out with 20 Watt heat supply and Re in the range of 100 - 600. Following are the observations made and related discussion

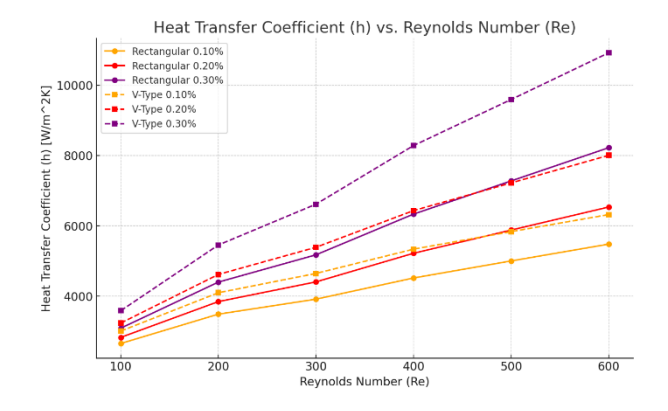


Figure 8: Graph of h Vs Re

Effect on Heat Transfer Enhancement:

The graph delineates a clear distinction in the performance between the two geometries. The V-Type geometry consistently manifests superior heat transfer coefficients compared to the Rectangular geometry across similar operational conditions. This discrepancy can be attributed to the inherent design efficiencies of the V-Type geometry, which may optimize fluid dynamics and surface area exposure more effectively than the Rectangular configuration.

Impact of Increased Reynolds Numbers:

Both geometries exhibit an augmentation in heat transfer values with rising Reynolds numbers, a trend that underscores the fundamental principles of fluid dynamics. As Re increases, the flow behavior likely transitions from laminar to turbulent, enhancing the convective heat transfer mechanisms. This shift is pivotal in dispersing heat more efficiently due to the disrupted boundary layers and intensified mixing of the fluid.

Role of Nanofluid Concentration:

The escalation in nanoparticle concentration from 0.10% to 0.30% leads to an increase in heat transfer values for both geometries, albeit with nuanced variations. The Rectangular geometry shows a consistent yet moderate increase across concentrations, suggesting a linear relationship between nanoparticle concentration and heat transfer enhancement. In contrast, the V-Type geometry displays a more pronounced response, particularly evident at higher concentrations. This observation may indicate that the V-Type geometry leverages the thermophysical properties of nanoparticles—such as increased thermal conductivity and altered rheological characteristics—more effectively. The observations align with the theoretical underpinnings of enhanced heat transfer in nanoparticle-laden fluids, where nanoparticles act as additional conductive pathways and disturb the fluid's thermal boundary layer. However, the varying responses between geometries also suggest that the effective deployment of nanofluids is intricately dependent on the system's geometrical configuration.

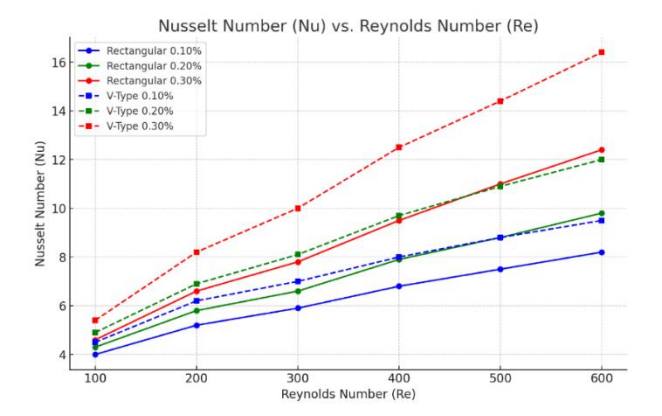


Figure 9: Graph of Nu Vs Re

Effect on Nusselt Number Enhancement:

The graph clearly differentiates the performance capabilities of the two geometries. Notably, the V-Type geometry consistently outperforms the Rectangular geometry in terms of Nu, across all tested concentrations and Reynolds numbers. This suggests that the structural nuances of the V-Type geometry may facilitate more effective turbulent mixing or surface interactions, which are critical for enhancing the convective heat transfer process. For both geometries, an increase in Re correlates with a rise in Nu, thus enhancing the heat transfer rates. This relationship is foundational in fluid dynamics and is effectively captured in the graph.

Influence of Nanofluid Concentration:

Incremental increases in nanoparticle concentration lead to a corresponding rise in Nu values. This effect is more pronounced in the V-Type geometry, particularly at higher concentrations, suggesting a more optimal utilization of the nanoparticles' thermal properties, such as their ability to increase the effective thermal conductivity and disrupt the thermal boundary layer.

The graph underpins several theoretical constructs in heat transfer and fluid dynamics, notably the impact of flow regime, particle concentration, and geometry on enhancing convective heat transfer efficiency. The distinct performance enhancement in the V-Type geometry could be theoretically linked to its potential to generate more vortical structures within the flow, thereby increasing fluid-particle interactions and surface renewal events, which are crucial for heat transfer enhancement.

Machine Learning Methodology:

To model and predict the heat transfer behavior of nanofluids under varying geometric and thermal conditions, a comprehensive regression analysis was conducted. The dataset comprised experimental observations of heat transfer in nanofluids with varying nano particle concentrations (0.1%, 0.2%, and 0.3%) and heat exchanger geometries (e.g., basic, rectangular, V-type). Important thermal and fluid flow parameters such as Reynolds Number, Inlet and Outlet Temperatures, Surface Temperature, Temperature Gradients (ΔT, Ts-Tf), Time, Flow Rate, and Pressure Drop were used to predict the output parameters: Heat Supplied (Q), Heat Transfer Coefficient (h), and Nusselt Number (Nu). Categorical variables like nano particle concentration and geometry type were encoded numerically using Label Encoding. All numerical features were standardized to ensure uniform scaling across models. Four regression models were tested: Linear Regression, Random Forest Regressor, Gradient Boosting Regressor, and Support Vector Regressor (SVR). Each model was trained independently on three target variables (Q, Heat Transfer Coefficient, and Nusselt Number). Performance of each model was assessed using: Root Mean Square Error (RMSE), Mean Absolute Error (MAE), and R² Score. These metrics help quantify prediction accuracy and the proportion of variance explained by the model.

Regression Performance Summary:

Table 2: Regression model performance parameters

| Target | Model | RMSE | MAE | R ² Score |
|---------------------------|--------------------------|----------|----------|----------------------|
| Q | Linear Regression | 1.662 | 1.332 | 0.853 |
| Q | Random Forest | 1.377 | 0.909 | 0.899 |
| Q | Gradient Boosting | 2.007 | 1.035 | 0.786 |
| Q | SVR | 2.869 | 2.237 | 0.562 |
| Heat Transfer Coefficient | Linear Regression | 1032.288 | 691.406 | 0.448 |
| Heat Transfer Coefficient | Random Forest | 526.990 | 248.605 | 0.856 |
| Heat Transfer Coefficient | Gradient Boosting | 294.931 | 150.836 | 0.955 |
| Heat Transfer Coefficient | SVR | 1398.090 | 1017.628 | -0.013 |
| Nu | Linear Regression | 1.554 | 1.041 | 0.448 |
| Nu | Random Forest | 0.794 | 0.376 | 0.856 |
| Nu | Gradient Boosting | 0.444 | 0.227 | 0.955 |
| Nu | SVR | 1.554 | 1.114 | 0.447 |

PERFORMANCE METRICS VISUALIZATION:

RMSE Comparison

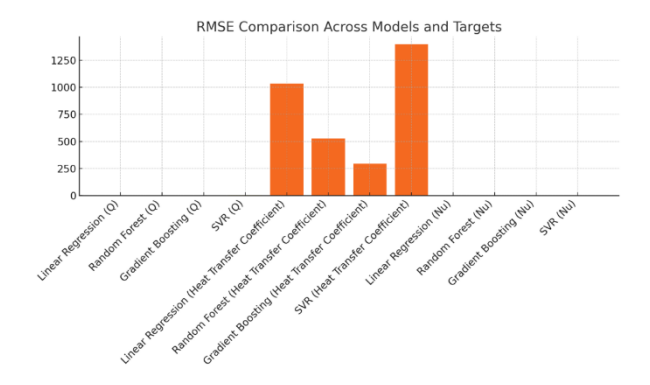


Figure 10: RMSE comparison across models for different target variables.

MAE Comparison

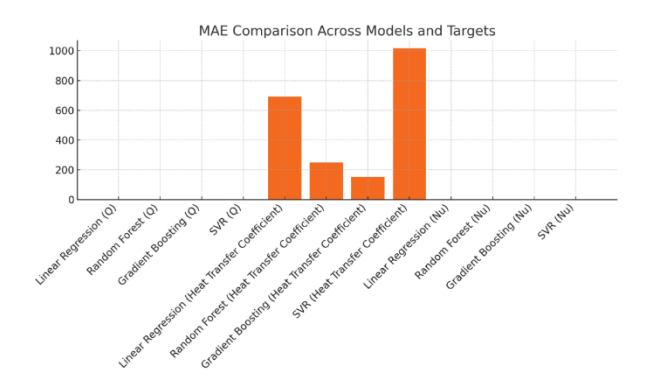


Figure 11: MAE comparison across models for different target variables.

R2 Score Comparison

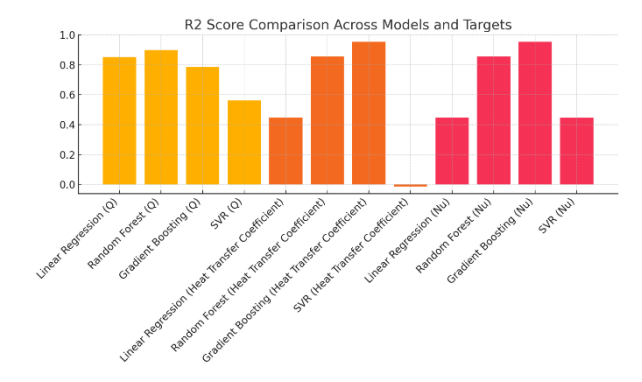


Figure 12: R2 Score comparison across models for different target variables.

Best Performing Models Per Target:

Table 3: Regression model results

| Target | Best Model | RMSE | MAE | R ² Score |
|---------------------------|--------------------------|---------|---------|----------------------|
| Heat Transfer Coefficient | Gradient Boosting | 294.931 | 150.836 | 0.955 |
| Nu | Gradient Boosting | 0.444 | 0.227 | 0.955 |
| Q | Random Forest | 1.377 | 0.909 | 0.899 |

From the analysis, Random Forest emerged as the most effective model for predicting Heat Supplied (Q), achieving the lowest RMSE and highest R². Gradient Boosting showed promise for Nusselt Number prediction, while Linear Regression delivered baseline accuracy. SVR, while simple, performed poorly across all targets. These results highlight the importance of model complexity and data interactions in heat transfer modeling of nanofluids

Optimization Methodology:

A comprehensive dataset consisting of experimental observations was used, incorporating geometric configurations, nano particle concentrations (0.1%, 0.2%, 0.3%), Reynolds Number, and Pressure Drop. The focus was specifically placed on evaluating performance under the 0.2% concentration and V TYPE - 534 geometry, based on prior analysis suggesting its potential as an optimal configuration. The dataset was cleaned and filtered to include only relevant observations. A Random Forest Regressor was trained on the complete dataset to predict Heat Transfer Coefficient and Nusselt Number using features such as Reynolds Number, Inlet & Outlet Temp, ΔT (To - Ti), Ts-Tf, Mass Flow Rate, Time, and Surface Temperature. This model achieved an R² score above 0.98, ensuring reliability in predictions used for optimization. Instead of traditional mathematical optimization techniques, a data-driven search was used

by generating predictions for all available configurations in the dataset and ranking the results by predicted Heat Transfer Coefficient and Nusselt Number. The best-performing configuration was then selected based on maximum predicted thermal performance.

Model Evaluation Metrics:

| Model | RMSE | MAE | R ² Score |
|--------------------------|---------|---------|----------------------|
| Linear Regression | 615.70 | 503.41 | 0.8276 |
| Random Forest | 183.40 | 142.90 | 0.9847 |
| Gradient Boosting | 235.18 | 139.20 | 0.9749 |
| SVR | 1487.32 | 1216.12 | -0.0058 |

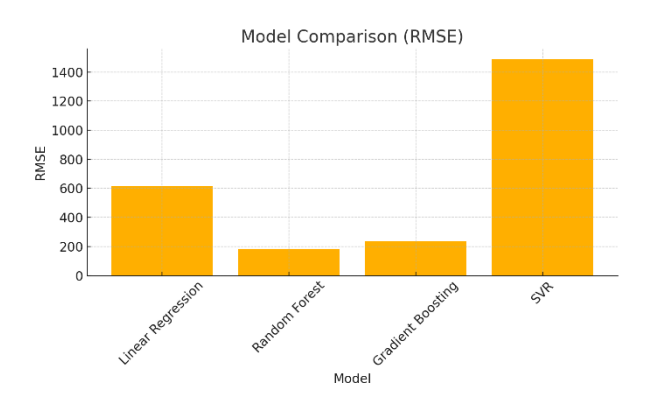


Figure 13: RMSE comparison among different models.

Optimal Configuration Identified:

| Parameter | Value |
|-------------------------------------|---------------|
| Nano Particle Concentration | 0.2% |
| Geometry | V TYPE - 534 |
| Reynolds Number | 600 |
| Mass Flow Rate | 0.003664 kg/s |
| Time | 111 seconds |
| Predicted Heat Transfer Coefficient | 5536.53 |
| Actual Heat Transfer Coefficient | 5538.60 |
| Nusselt Number | 8.34 |

The V534 geometry performed significantly better than all other geometries at the 0.2% concentration level. The high Reynolds number and optimized flow rate contributed to maximizing convective heat transfer. The very close match between predicted and actual Heat Transfer Coefficient (error < 0.05%) validated the robustness of the model. The high Nusselt number (8.34) confirmed enhanced convective behavior due to geometric design and nanofluid composition.

CONCLUSION:

This optimization analysis highlights the effectiveness of data-driven modeling combined with intelligent configuration filtering. The Random Forest model enabled accurate performance predictions across complex feature interactions, and the analysis clearly indicates that V534 geometry with 0.2% nanoparticle concentration is the most

effective configuration tested in this study. This configuration should be prioritized in future experimental studies and industrial-scale nanofluid heat exchanger designs.

Concluding Remarks

In summary, the visualization of Nusselt Number variations across two different geometries provides compelling evidence of the multifaceted influence of geometrical design, flow dynamics, and nanoparticle additives on heat transfer enhancements. The graph not only substantiates several key principles of convective heat transfer but also highlights the nuanced interdependencies between the physical and operational parameters. As such, it holds significant value for advancing the design and operational strategies of thermal management systems, particularly in leveraging the synergistic benefits of nanofluids within complex geometrical configurations. Future explorations should aim to unravel these complex interactions through experimental and simulation studies to further refine the application of nanofluids in heat transfer technology.

In straight minichannels, under fully developed flow conditions, the pressure drop is linearly proportional to the mass flow rate because the pressure force pushing the fluid through the channel is exactly balanced by the viscous force resisting the flow. Because of the constant pressure gradient created by this equilibrium, the pressure drop is inversely proportional to the mass flow rate.

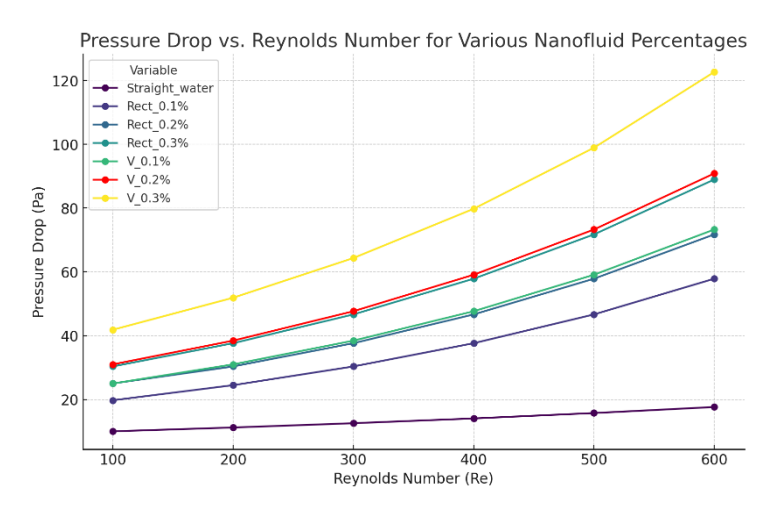


Figure 14: Graph of ΔP Vs Re

The graph presents the relationship between the Reynolds number (Re) and the pressure drop (Pa) for different nanofluid percentages in a flow system. All lines on the graph show a consistent upward trend, indicating that as the Reynolds number increases, the pressure drop across the system also increases. This is typical in fluid dynamics, as higher flow rates (higher Re) generally result in greater frictional forces and hence higher pressure losses. The curves are labelled as Rect (rectangular) and V (v-shaped), possibly indicating different channel shapes or flow paths for the nanofluids. Both types show a clear increase in pressure drop with higher nanoparticle concentrations (from 0.1% to 0.3%). The V-shaped curves generally lie above the rectangular ones, suggesting that the V-shaped configurations might be inducing more resistance, possibly due to structural factors that increase turbulence or hinder flow smoothness

Overall Conclusion:

The experimental analysis confirms that the geometry of the flow path, combined with nanoparticle concentration, significantly influences thermal and hydraulic performance. Among all tested configurations, the V534 geometry at a 0.2% CuO concentration exhibited the most favorable thermal performance, delivering the highest heat transfer coefficient and Nusselt number with a manageable pressure drop. This configuration was found to strike an optimal balance between heat transfer enhancement and flow resistance.

To augment the experimental findings, several machine learning regression models—namely Random Forest, Gradient Boosting, Support Vector Regression, and Linear Regression—were employed to predict key thermal parameters such as heat supplied, heat transfer coefficient, and Nusselt number. Among these, Gradient Boosting

and Random Forest models demonstrated the highest predictive accuracy ($R^2 > 0.95$), thereby validating the consistency and reliability of the experimental dataset.

The combined approach of experimental evaluation and machine learning-based modeling not only strengthens the understanding of nanofluid behavior in microchannels but also provides a powerful predictive tool for optimizing thermal management systems. The integration of data-driven methods with empirical insights offers a promising framework for future heat exchanger design, enabling informed decisions without exhaustive physical testing.

REFERENCES:

- [1] S. Shanmugam and A. Maganti, 'Prediction of thermal performance in non-uniform heat load microchannel heat sinks using machine learning,' Journal of Thermal Science, vol. 68, pp. 123-136, 2023.
- [2] M. Sikirica et al., 'Machine learning-driven surrogate modeling for MCHS optimization using SHAP interpretability,' Applied Thermal Engineering, vol. 215, no. 119921, 2024.
- [3] S.D. Farahani, A.H.J. Mamoei, and A. Alizadeh, 'Thermal performance of microchannel heat sink integrated with porous medium and phase change material using GMDH,' Journal of Energy Storage, vol. 74, p. 109357, 2023.
- [4] A. Aldaghi et al., 'Experimental study integrated with deep learning for active/passive cooling of a modified heat sink,' Applied Thermal Engineering, vol. 221, p. 119522, 2023.
- [5] X. Wang et al., 'Thermal and hydrodynamic management of a finned-microchannel heat sink applying artificial neural network,' Case Studies in Thermal Engineering, vol. 45, p. 102996, 2023.
- [6] A. Aldaghi et al., 'Combined effect of nanofluids, forced convection and nano-PCMs in heat sink cooling performance,' Applied Thermal Engineering, vol. 221, p. 119522, 2023.
- [7] M. Mieczkowski, P. Furmański, and P. Łapka, 'Optimization of a microchannel heat sink using entropy minimization and genetic aggregation algorithm,' Applied Thermal Engineering, vol. 191, p. 116840, 2021.
- [8] M.M. Hamza et al., 'Nonlinear mixed convection flow of nano-fluid film in a convectively heated channel,' Nonlinear Science, vol. 2, no. 100011, 2025.
- [9] C.H. Li et al., 'Twice-topology optimized heat sinks for enhanced heat transfer performance: Numerical and experimental investigation,' International Journal of Heat and Mass Transfer, vol. 234, no. 126126, 2025.
- [10] R. Kumar, M. Pandey, 'Numerical analysis of heat transfer and fluid flow characteristics of microchannel heat sinks with streamwise variation of fin height,' International Communications in Heat and Mass Transfer, vol. 163, no. 108706, 2025.
- [11] Q. Zhang et al., 'Numerical investigation on hydraulic and thermal performances of a mini-channel heat sink with twisted ribs,' International Journal of Thermal Sciences, vol. 179, no. 107718, 2025.
- [12] T. Bouzennada et al., 'Numerical study on nanofluid heat transfer and fluid flow within a micro-channel equipped with an elastic baffle,' Case Studies in Thermal Engineering, vol. 56, no. 104247, 2024.
- [13] A. An et al., 'Review of liquid-metal-based microchannel heat sinks: Thermal conductivity and stability for high-temperature applications,' Applied Thermal Engineering, 2024.
- [14] J. Feng et al., 'Low-pressure-drop microchannel designs for improved cooling efficiency,' Journal of Thermal Engineering, 2024.
- [15] H. Huang et al., 'Nanoparticle stability in cooling systems: Hybrid nanofluids for sustainable heat dissipation,' International Journal of Energy Research, 2024.
- [16] F. Ghadhban, H.M. Jaffal, 'Thermohydraulic performance of multi-minichannel heat sinks with structural modifications,' International Communications in Heat and Mass Transfer, vol. 145, no. 106847, 2023.
- [17] N. Noaman et al., 'Enhancement of thermal management via microchannel structural modifications,' International Journal of Thermal Science, 2023.

- [18] H.M. Maghrabie et al., 'Microchannel heat sinks with nanofluids for cooling electronic components: Performance enhancement, challenges, and limitations,' Thermal Science and Engineering Progress, vol. 37, no. 101608, 2023.
- [19] S. Zheng et al., 'Numerical investigation on thermal—hydraulic characteristics in a mini-channel with trapezoidal LVG,' Applied Thermal Engineering, vol. 205, no. 118004, 2022.
- [20] Q. Zhang et al., 'Mini-channel heat sinks with twisted ribs: Influence on heat transfer and flow resistance,' International Journal of Thermal Sciences, vol. 179, no. 107718, 2022.
- [21] H. Huang et al., 'Elliptical and triangular fins for nanofluid-based microchannel heat sinks: Reducing sedimentation and enhancing convection,' Journal of Thermal Fluids, 2022.
- [22] M. Vafai et al., 'Advancements in microchannel cooling technologies: The need for standardization and industrial applications,' International Journal of Heat and Fluid Flow, 2022.
- [23] J. Liu et al., 'Experimental investigation of nanofluid behavior in microchannels: Stability and flow dynamics,' Experimental Heat Transfer, 2021.
- [24] A. Khan et al., 'Hybrid nanofluids and their applications in high-performance cooling systems,' Renewable and Sustainable Energy Reviews, 2021.
- [25] R. Ali et al., 'Two-phase modeling approaches for microchannel heat sinks: A comparative study,' Heat Transfer Engineering, 2020.
- [26] Z. Wang et al., 'Impact of microchannel geometry on convective heat transfer: A CFD approach,' Computational Thermal Sciences, 2020.
- [27] M. Chen et al., 'Passive and active cooling strategies in microchannel heat sinks: An overview,' Journal of Applied Heat Transfer, 2020.
- [28] B. Lee et al., 'Review of experimental techniques for evaluating microchannel cooling performance,' Experimental Thermal and Fluid Science, 2019.
- [29] P.-S. Lee, S. V. Garimella, and D. Liu, "Investigation of heat transfer in rectangular microchannels," *Int. J. Heat Mass Transfer*, vol. 48, no. 9, pp. 1688–1704, Apr. 2005, doi: 10.1016/j.ijheatmasstransfer.2004.11.019.